THE RIGAKU JOURNAL
VOL. 22 / NO. 1 / 2005, 16–25

ANALYZING MICROSTRUCTURE BY RIETVELD REFINEMENT*

DAVOR BALZAR[1,2,**] AND NICOLAE C. POPA[3,4]

[1] *Department of Physics & Astronomy, University of Denver, Denver, CO 80208, U.S.A.*
[2] *Materials Science and Engineering Laboratory, National Institute of Standards and Technology, Boulder, CO 80305, U.S.A.*
[3] *Joint Institute for Nuclear Research, Dubna, Moscow Region, Russia*
[4] *National Institute for Materials Physics, P.O. Box MG-7, Bucharest, Romania*

Rietveld refinement has a primary purpose of refining crystal structure. However, this powerful technique is being increasingly used for obtaining microstructural information, such as texture, average domain size and crystallite size distribution, strain and stress, and crystalline defect concentration. This review discusses the determination of these properties with a particular emphasis on the modeling of diffraction-line broadening and diffraction-line shift in current Rietveld-refinement programs. A few examples are given and limitations of the model illustrated on a case of "super-Lorentzian" line shapes.

1. Introduction

Since its inception over 35 years ago, Rietveld refinement (Rietveld, 1969) has come a long way. In the beginning, the aim was to carry out crystal-structure refinement using neutron diffraction. As its primary purpose was refinement of the perfect crystal structures of polycrystalline samples, there was a need to introduce corrections to peak intensities and positions, as calculated for a perfect powder standard, in order to match experimental patterns affected by sample texture and defects (*i.e.* residual or microscopic strains/stresses, crystal defects, small coherently diffracting domain size, *etc.*). It was not until the 1990s that an effort was made to determine microstructural properties through Rietveld refinement. Popa (1992) worked out a procedure for texture determination by the generalized spherical harmonics, which was implemented into GSAS (Larson & Von Dreele, 2001) by Von Dreele (1997). Furthermore, an anisotropic line-broadening modeling for arbitrary crystal symmetry was proposed independently by Popa (1998) and Stephens (1999) which was implemented shortly thereafter into most major Rietveld programs. Peak shifts were used for the residual strain/stress determination by Ferrari & Lutterotti (1994), Daymond *et al.* (1997) and Balzar *et al.* (1998). Next, an interest in determining an accurate crystallite size distribution led to work on introducing several common size distributions (*i.e.* lognormal, gamma, *etc.*) into Rietveld refinement and similar full-powder-pattern approaches (Krill & Biringer, 1998; Langford *et al.*, 2000; Popa & Balzar, 2002). Recently, attempts are being made to include modeling of crystal defects and dislocation configurations (Ungár, 2001; Scardi & Leoni, 2002). These developments gave us new tools for assessing the microstructure and thus a complete characterization of samples. Although the main intention of these models is to allow the determination of microstructural properties, in general, they are more robust over earlier approaches that were devised only to correct for undesirable effects, such as relative peak intensity changes due to texture or anisotropic peak broadening due to strain effects.

The aim here is to review the modeling of microstructural properties in Rietveld refinement and to contrast it with a traditional approach for evaluating microstructural properties. A few examples in the determination of the crystallite size distribution and residual strain and texture will be given, in order to illustrate some of the possibilities. This is not meant to be an exhaustive review of the topic, as the main intent is to focus on our previous work. Moreover, the microstructural applications of Rietveld refinement are quickly developing into a powerful tool with a broad range of physical effects that are being modeled, which would be hard to cover in detail here.

2. Microstructure Modeling in Rietveld Refinement

Microstructural effects can broadly be classi-

** Corresponding author. Web: www.du.edu/~balzar; E-mail: balzar@du.edu

fied in three types as affecting relative intensities of the diffraction lines (that is, deviation from the intensities as calculated for a randomly oriented powder due to texture), positions of diffraction lines (mainly caused by residual stresses present in the bulk sample), and widths of diffraction lines (mainly caused by small coherently diffracting domain size and lattice strains due to crystal defects). However, some of the crystal defects, for instance extrinsic stacking faults and twins, can affect both the diffraction line width and position, making any general modeling of these effects in Rietveld-refinement programs challenging. We will discuss each in turn, but focus in particular on diffraction-line broadening and diffraction-line shift.

2.1. Texture

A simple correction for preferred orientation was included in the Rietveld refinement from the beginning (Rietveld, 1969). Later, the March-Dollase model (Dollase, 1986) was extensively used in Rietveld-refinement programs. Both approaches were only capable of correcting for effects of uniaxial preferred orientation in sample, and were not robust to handle cases of strong texture or capable of modeling more complicated textures. Popa (1992) proposed the model for the determination of texture in terms of generalized spherical harmonics for all Laue classes, which was adopted in GSAS by Von Dreele (1997) and independently developed by Matthies *et al.* (1997). Nowadays, the spherical harmonics model is used for texture determination in practically all major Rietveld-refinement programs. For methodology, the readers are directed to the ample literature on the subject. An example is given later in this article in connection with the determination of residual stress in cold-rolled uranium plate.

2.2. Diffraction-line Broadening

If we denote the instrumental, physical, and observed profile by $g(x)$, $p(x)$ and $h(x)$, respectively, the observed Bragg profile is given by a convolution integral:

$$h(x) = \int p(z)g(x-z)dz + b(x) + n(x) \qquad (1)$$

where $b(x)$ is the background and $n(x)$ the noise ($\langle n(x)\rangle = 0$). The physical profile itself is a convolution of size-broadened and strain-broadened profiles (for physical origins and more detailed classifications, see, for instance, Balzar (1999)).

Rietveld refinement was originally developed for refinement of crystal structures from neutron powder diffraction data (Rietveld, 1969). Because of the available neutron flux and instrumentation at that time, intrinsic (instrumental) resolution was generally poor. That is, for most samples, instrumental broadening gave a dominant contribution to line broadening and sample-related (physical) broadening was masked by it in most cases. As a result, the instrumental contribution to the line broadening gave an overall Gaussian observed diffraction line profile. With the advent of modern laboratory X-ray powder diffractometers and particularly synchrotron radiation and instrumentation, a significantly better resolution was obtained which resulted in a much narrower intrinsic line profile. Moreover, the observed line profile could not be fit by a Gauss function but rather with some combination of Gauss and Lorentz (Cauchy) functions. In general, such combinations in use are Voigt function (convolution of Gauss and Lorentz functions), pseudo-Voigt (weighted sum of the two), and Pearson VII functions (generalized Lorentz function with a variable exponent). For a definition and additional information about particular functions for fitting diffraction lines, see for instance, Howard & Preston (1989) and Balzar (1999). Nowadays, the most widely used in Rietveld refinement programs is generalized Thompson, Cox & Hastings (1987) (TCH) pseudo-Voigt model for diffraction line profiles:

$$\Gamma_G^2 = U\tan^2\theta + V\tan\theta + W + P/\cos^2\theta \qquad (2)$$

$$\Gamma_L = X/\cos\theta + Y\tan\theta + Z \qquad (3)$$

Here, Γ is the full width at half maximum (FWHM) of the line profile, U, V, W, X, Y, and Z are refinable parameters and L and G denote Lorentz and Gauss profiles, respectively. Equation (2) is based on the Caglioti *et al.* (1958) article, which modeled neutron-diffraction line shapes in terms of collimator and monochromator transmission functions in Gaussian approximation. The last term in (2) was added by Young & Desai (1989) and describes Gaussian contribution to the Scherrer (1918) size broadening:

$$\beta_S = \frac{\lambda}{D_V\cos\theta} \qquad (4)$$

where S denotes size, λ is the wavelength and D_V the volume-averaged domain size (apparent dimension in the direction normal to the reflecting planes). The other measure of domain size is based on the Fourier analysis of the line pro-

file and gives the area-averaged apparent dimension (column length) in the direction normal to the reflecting planes, D_A (Bertaut, 1949). These two crystallite size dimensions are called "apparent" because they only relate to the real average crystallite dimension.

Equation (3) is the Lorentzian line width and includes contributions from Lorentzian size broadening *X*, Lorentzian strain broadening *Y* and a constant *Z*. *Z* is customary set to zero in most Rietveld-refinement programs.

The term that varies with $\tan\theta$ stems from Stokes & Wilson (1944) definition of maximum (upper limit) of strain:

$$e = \frac{\beta_D}{4\tan\theta} \tag{5}$$

where D denotes distortion (strain).

Because a convolution of any number of Voigt functions is also a Voigt function, the TCH model implicitly assumes that the observed, size-broadened, and strain-broadened line profiles are Voigt functions (Balzar & Ledbetter, 1995). Hence, it is easy to recognize from (2) and (3) that parameters *X* and *P* will relate to size broadening and *Y* and *U* to strain broadening. However, some instrumental contributions have similar dependence on diffracting angle and that contribution has to be carefully separated to obtain accurate information about domain size and strain from line broadening (see Balzar *et al.* (2004) for procedures involving both X-ray and neutron sources).

Therefore, to obtain a physical contribution to the broadening, it is sufficient to refine four parameters in equations (2) and (3). Before estimating physical broadening of a sample under investigation (sam), these refined values have to be corrected for instrumental effects, which are determined by refinement of line profiles of the "standard" sample (stand). We can write

$$\Gamma_{\text{eff}} = \Gamma_{\text{sam}} - \Gamma_{\text{stand}} \tag{6}$$

where Γ stands for *X*, *P*, *U*, and *Y*. The effective value (eff) depicts the pure physically broadened profile parameters.

As the parameters in equations (2) and (3) are FWHMs, they should be converted to integral breadths of size-broadened and strain-broadened profiles before calculating associated domain size and strain values. Conversion factors are (Langford, 1978):

$$\frac{\beta_L}{\Gamma_L} = \frac{\pi}{2}, \quad \frac{\beta_G}{\Gamma_G} = \frac{1}{2}\sqrt{\frac{\pi}{\ln 2}} \tag{7}$$

where Γ_L and Γ_G are calculated from the effective parameters determined using (6). However, GSAS internally reduces Gauss FWHM by a factor of $(8\ln 2)^{1/2}$ (Larson & Von Dreele, 2001); thus the second equation in case of GSAS is

$$\frac{\beta_G}{\Gamma_G} = \sqrt{2\pi} \tag{8}$$

Then, the Lorentz and Gauss integral breadths are combined for both size and strain parts according to the relation (Langford, 1978):

$$\beta_i = (\beta_G)_i \frac{\exp(-k^2)}{1-\text{erf}(k)}; \quad k = \frac{\beta_L}{\sqrt{\pi}\,\beta_G} \tag{9}$$

where *i* stands for S and D. Only now can β_S and β_D be related to the corresponding values of D_V and *e*, according to equations (4) and (5).

The conversions (7) are equivalent to the alternative numerical expressions connecting the integral breadth β and FWHM Γ of a pseudo-Voigt profile, as it is customary used in Rietveld-refinement programs (Thompson *et al.*, 1987).

There is no *a priori* reason to believe that a simple (pseudo) Voigt model, discussed here, can successfully describe all size and strain broadening-related effects because these profiles may correspond only to very special cases of size and strain broadening. A better approach may be to use line profiles derived from physical models. Recently, there have been attempts to model broadening in Rietveld refinement and other full-powder-pattern-fitting programs (FPPF) in terms of physically meaningful parameters, such as crystallite size distribution and dislocation density and other related parameters (Scardi & Leoni, 2001, 2002; Ungár *et al.*, 2001 and references therein). Still, Rietveld refinement is a difficult setting to account for all the physical reasons for line broadening and other effects on diffraction lines; many physical origins affect diffraction lines in a similar manner as a function of diffraction angle thus implying a high degree of correlation between different refinable parameters. Therefore, without additional independent information about the nature and abundance of crystal defects present in a particular sample under investigation, it is difficult to assess reliability of results obtained. However, a general Voigt-based model, as currently available in most major Rietveld refinement programs, at least gives some results that can be *a posteriori* related to a correct physical model in case the additional information becomes available.

In the next section, we compare the determi-

nation of the lognormal size distribution of spherical crystallites through both direct refinement of size-distribution parameters and indirectly through the Rietveld refinement on an example of CeO_2 powder.

2.2.1. Determination of Crystallite Size Distributions

The second derivative of the size Fourier coefficients is related to the column-length distribution function (Guinier, 1963; Warren 1969). Presuming an identical shape for all crystallites, the column-length distribution function can be calculated as an integral with a variable limit over the crystallite distribution function (Smith, 1976). Determination of the real crystallite size distribution then includes the third derivatives of the size Fourier coefficients, which further amplifies already large initial errors of the experimental Fourier coefficients. Additionally, Fourier coefficients for large harmonic numbers are unreliable because of approximations inherent to the size-strain separation approaches (see again Warren (1969) and Klug & Alexander (1974)). However, if one assumes a certain size distribution of crystallites in a sample, it is possible to relate both volume-averaged and area-averaged domain size calculated for that distribution to the original distribution parameters and calculate the latter based on the results of refinement of the former. This procedure was first proposed by Krill & Birringer (1998) and later discussed by Langford *et al.* (2000) and Popa & Balzar (2002) for lognormal distribution. The gamma distribution is another bell-shaped distribution that was used to describe the distribution of crystallite sizes (York, 1997; Scardi & Leoni, 2001) or crystalline defects (Berkum, 1994). It was discussed in a similar way elsewhere (Popa & Balzar, 2002).

The lognormal distribution for spherical crystallites is characterized by two parameters, the average radius $\bar{R}$ of the particles and the dispersion σ_R^2. It is convenient to define a dimensionless ratio (Popa & Balzar, 2002)

$$c=\sigma_R^2/\bar{R}^2 \tag{10}$$

to characterize the distribution. Then the lognormal distribution can be written as follows:

$$f(R)=R^{-1}[2\pi\ln(1+c)]^{-1/2} \times\exp\{-\ln^2[R\bar{R}^{-1}(1+c)^{1/2}]/[2\ln(1+c)]\} \tag{11}$$

One can calculate the volume-averaged and area-averaged dimensions as (Popa & Balzar, 2002):

$$D_V=3\bar{R}(1+c)^3/2\,,\quad D_A=4\bar{R}(1+c)^2/3 \tag{12}$$

These two equations can be used to determine the parameters of lognormal size distribution, $\bar{R}$ and c, if D_V and D_A are obtained from Rietveld refinement.

The size-broadened profile resulting from the lognormal size distribution of spherical crystallites can be expressed as follows:

$$\bar{P}(s)=(3\bar{R}/2)(1+c)^3\bar{\Phi}(2\pi s\bar{R}) \tag{13}$$

$$\bar{\Phi}(x)=\pi^{-1/2}\int_{-\infty}^{\infty}dt \times\exp(-t^2)\Phi\{x(1+c)^{7/2}\exp[t(2\ln(1+c))^{1/2}]\} \tag{14}$$

where

$$\Phi(x)=(x^2+\sin^2 x-x\sin 2x)/x^4 \tag{15}$$

is an interference function for a sphere. This expression cannot be calculated analytically either in direct or Fourier space. As this calculation is computer-time intensive, a simple approximation was proposed (Popa & Balzar, 2002):

$$\bar{\Phi}(x)=(8/3)(1+c)^{-3} \times\left\{\eta_1 a_1^{-1}(1+4x^2/a_1^2)^{-1}+\eta_2 a_2^{-1}(1+4x^2/a_2^2)^{-1} +(1-\eta_1-\eta_2)a_3^{-1}\begin{cases}\exp(-4x^2/\pi a_3^2) & \text{for } c\le 1\\ (1+4x^2/a_3^2)^{-1} & \text{for } c>1\end{cases}\right\} \tag{16}$$

The parameters η_1, a_1, η_2, a_2 ($0\le\eta_i\le 1$) can be freely adjusted during the fit but a_3 has to be constrained to conserve the integral breadth of the exact profile:

$$a_3=(1-\eta_1-\eta_2)/[3(1+c)^3/8-\eta_1/a_1-\eta_2/a_2] \tag{17}$$

The parameters η_1, a_1, η_2, a_2 can be fitted by empirical analytical functions in c:

$$\eta_1(c)=0.25631+0.018638c+0.001155c^2 +3.5671c\exp(-2.0467c^{0.93346}) \tag{18}$$

$$a_1(c)=4.02326\exp(-44.6429c) +3.13982\exp(-7.01128c) +0.580742\exp(-0.413958c) +0.381245\exp(-1.10827c) \tag{19}$$

$$\eta_2(c)=\begin{cases}0 & \text{for } c\le 0.4\\ 0.59951-0.020058(c-0.4) & \\ -0.45347/[1+3.3933(c-0.4)^2] & \\ -0.14604\exp[-0.49272(c-0.4)^2] & \text{for } c>0.4\end{cases} \tag{20}$$

Table 1. Results of the fit by a model assuming a lognormal size distribution of spherical crystallites: The first moment of the distribution $\bar{R}$, the ratio of the distribution dispersion to the first moment $c=\sigma_R^2/\bar{R}^2$, and the corresponding volume-averaged D_V domain size. Results of the Rietveld refinement are also given for comparison: Volume-averaged domain size D_R and strain e. The last column gives values of D_R when strain-related parameters were forced to yield a zero strain.

	$\bar{R}$ (Å)	c	D_V (Å)	D_R (Å)	e (10^{-4})	D_R (Å) for $e=0$[1]
Birmingham	89.0 (10)	0.187 (5)	223 (5)	227 (3)	0	227 (3)
Le Mans	90.9 (3)	0.188 (2)	229 (2)	235 (2)	2.2 (1)	224 (1)
ESRF	90.0 (10)	0.192 (6)	229 (6)	223 (1)	1.5 (1)	219 (1)
NSLS	93.3 (7)	0.177 (3)	228 (4)	236 (2)	2.3 (1)	224 (1)
ILL	93.0 (20)	0.173 (7)	225 (9)	221 (3)	0.1 (3)	220 (2)
NIST	93.0 (40)	0.184 (15)	232 (19)	231 (6)	4.5 (8)	216 (4)
ISIS	91.0 (10)	0.191 (4)	231 (5)	232 (1)	5.5 (2)	224 (1)

[1] Strain-related parameters set to the values of the instrumental standard sample during the refinement.

$$a_2(c)=0.32781[1+1.5399(c-0.4) -0.21223(c-0.4)^2+0.18158(c-0.4)^3]^{-1} \quad (21)$$

From (20), $\eta_2(c)=0$ for $c\leq 0.4$. Therefore, from (16) it follows that the pseudo-Voigt function is a satisfactory approximation for the size-broadened profile only for $c\leq 0.4$. For higher value of c a second Lorentz function must be added. Its weight increases with increasing c and the weight of the Gauss component decreases. For $c\approx 1$, the profile is well approximated by a sum of two Lorentz functions. A third Lorentz function must be added for $c>1$. For $c>6$, even three Lorentz functions are not enough for a satisfactory fit, but it is highly unlikely to find samples with such a large dispersion of crystallite sizes.

From this discussion, it is evident that the size-broadened profile can be approximated by the pseudo-Voigt function, that is, the TCH model used in Rietveld-refinement programs, only for samples that follow the lognormal size distribution of the crystallites with a limited dispersion in the region $0\leq c\leq 0.4$. From (12), it follows that the ratio $D_V/D_A=(9/8)(1+c)$ can therefore take values in the range from 1.125 to ∞. The size-broadened profile is very often modeled by the Voigt function. In order for the column-length distribution function to always be positive, it was found (Balzar & Ledbetter, 1993) that an assumed size-broadened Voigt function requires the ratio of volume-averaged and area-averaged domains to be in the range:

$$(2\pi e)^{1/2}\,\mathrm{erfc}(1/2^{1/2})\approx 1.31\leq D_V/D_A<2 \quad (22)$$

The lower limit of this ratio constraints the dispersion parameter to $c\geq 0.164$. Therefore, the Voigt function appears to be an inadequate approximation for both very sharp and broad lognormal distributions of spherical crystallites. However, these additional restrictions are not placed on a pseudo-Voigt function, which indicates that the latter might be a better approximation for the size-broadened profile for samples with narrow crystallite-size distributions.

2.2.2. Application to CeO_2 Powders

We present here a comparison of results obtained by assuming physical model (lognormal size distribution of spherical crystallites) and the phenomenological approach using Rietveld refinement. Both methodologies were applied on the measurements collected at seven different instruments on the CeO_2 powder sample prepared for the IUCr Commission on Powder Diffraction (CPD) Size-Strain Round Robin (see Balzar *et al.* (2004) and Audebrand *et al.* (2000)). Table 1 shows the results obtained for the lognormal size distribution, where the parameters of the lognormal distribution were fitted directly through the least-squares refinement. A Gaussian function was also included to model strain broadening; however, the addition of this strain-related parameter did not significantly improve the fit. Volume-averaged domain size was calculated from (12) for comparison with the results obtained by Rietveld refinement, following (4), (6), and (9). All the data sets, except Birmingham laboratory X-ray data, yielded a relatively small strain contribution. If the strain-related parameters are set to give zero strain, volume-averaged domain sizes agree even better with the results obtained by the direct fit of lognormal size distribution parameters.

Examples when Rietveld refinement fails to successfully fit a diffraction pattern were given previously (Young & Desai, 1989), and were attributed to the "super-Lorentzian" line profiles that cannot be fitted with Voigt and related

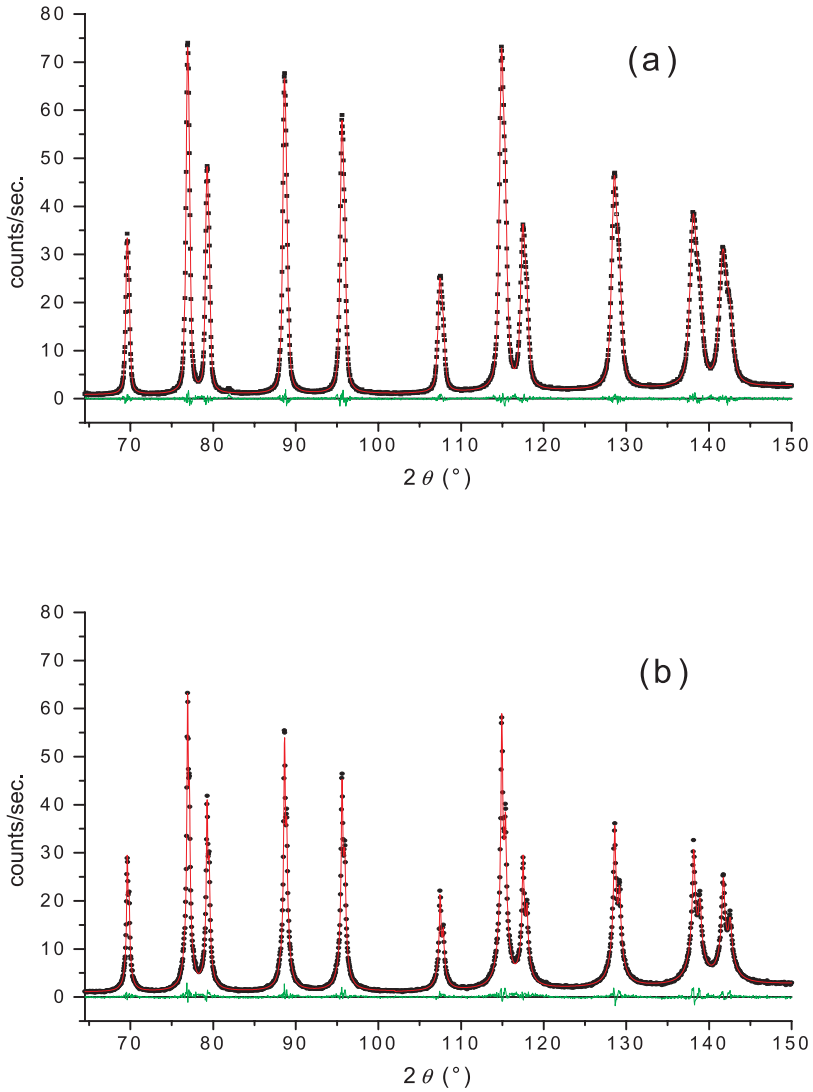

Fig. 1. The powder pattern fitted with the size-broadened profile calculated for the lognormal distribution: (a) Size Strain Round Robin CeO_2 sample: R_{wp}=0.0390; (b) Commercial CeO_2 powder: R_{wp}=0.0477.

functions used in Rietveld refinement programs. Popa & Balzar (2002) reported that a commercial CeO_2 powder gave "super-Lorentzian" line profiles. Figure 1 compares that diffraction pattern with the pattern given by the Size Strain Round Robin CeO_2 sample. The latter sample shows "regularly" broadened lines with $K\alpha_1$ and $K\alpha_2$ overlapped at high angles (Fig. 1a), which can be successfully fitted by the Voigt function or its approximations, while the former sample exhibits "super-Lorentzian" profiles, with long tails and $K\alpha_1$ and $K\alpha_2$ separated at high angles (Fig. 1b). Although the "super-Lorentzian" profiles could not be successfully fitted with a single Voigt or related function, an assumed lognormal size distribution of spherical crystallites gave an excellent fit. Table 2 illustrates the difference in parameters of the lognormal size distribution for two cases: "super-Lorentzian" profiles yield a large c ratio that indicates a broad distribution with a large fraction of small crystallites and large ratio of volume-averaged to area-averaged domain size

Table 2. The results of the fit of an *a priori* lognormal size distribution for the Size Strain Round Robin CeO_2 sample (S1) and commercial CeO_2 sample (S2): The average radius $\bar{R}$, volume-averaged D_V, and area-averaged D_A apparent domain sizes.

Sample	$\bar{R}$ (Å)	c	D_V (Å)	D_A (Å)
S1	89.7 (6)	0.181 (4)	222 (3)	167 (2)
S2	16.8 (2)	2.820 (2)	1408 (14)	328 (3)

($D_V/D_A \approx 4.3$) as opposed to about 1.3 for the Size Strain Round Robin sample.

2.3. Diffraction-line Shifts

Residual stresses will in general result in anisotropic diffraction-line shifts of different Bragg reflections. Thus, an analysis of interplanar d spacings as a function of direction in the sample (the so-called "$\sin^2\psi$" technique, Hauk (1952); Christenson & Rowland (1953)), can be used to evaluate strains and stresses (for details see, for instance, Noyan & Cohen (1987); Hauk (1997)). An alternative approach was proposed (Ferrari & Lutterotti, 1994; Daymond *et al.*, 1997; Balzar *et al.*, 1998; Popa & Balzar, 2001), which includes the refinement of strain and stress related parameters in the Rietveld refinement program. An advantage of this approach is that all available Bragg reflections are used simultaneously to obtain the strain tensor. Even if the strain/stress determination is not of interest, diffraction line shifts caused by residual stresses will generally be crystal-direction dependent. These diffraction line shifts should be corrected for, in order to carry out an accurate refinement using the Rietveld approach.

Very few Rietveld programs are able to handle the analysis of peak shifts to obtain strain and/or stress; notable exceptions are MAUD (Lutterotti, 1998) and GSAS (Larson & Von Dreele, 2001). In GSAS, both isotropic $\varepsilon_{ph,i}$ and anisotropic $\varepsilon_{ph,a}$ components of strain can be determined from the neutron time-of-flight (TOF) measurements, through the peak shift from the diffraction-line maximum T_{ph}, where p denotes a particular phase and h a particular histogram (diffraction pattern):

$$\Delta T_{ph} = (T - T_{ph}) - \varepsilon_{ph,i} d_p - \varepsilon_{ph,a} d_p \Gamma \tag{23}$$

Here, TOF T extends over each diffraction-line point and Γ is the orientation parameter defined for cubic crystal symmetry as

$$\Gamma_C = \frac{h^2k^2 + k^2l^2 + l^2h^2}{(h^2 + k^2 + l^2)^2} \tag{24}$$

and for hexagonal crystal symmetry as

$$\Gamma_H = \frac{l^2}{\frac{4}{3}\frac{c^2}{a^2}(h^2 + hk + k^2) + l^2} \tag{25}$$

where a and c denote lattice parameters and hkl Miller indices. Γ varies from 0 for {h00} to 1/3 for {hhh} for cubic symmetry and is zero for {hk0} for hexagonal symmetry.

The expressions for Γ assume constant stress in all grains of polycrystalline material (Reuss, 1929 approximation). Recently, a different approach was proposed (Wang *et al.*, 1999, 2000; Behnken, 2000) that does not require Reuss (1929) or other assumption. It relies on a modeling of strain orientation distribution function (SODF) in terms of generalized spherical harmonics, that is, similar to the determination of texture through the crystallite orientation distribution function (CODF) (Bunge, 1982). However, for a successful application in the Rietveld refinement, the challenge lies in the accurate modeling of strain and stress dependence on the crystallographic direction and the ability to handle arbitrary crystal symmetry. In a recent paper, Popa & Balzar (2001) presented a method for modeling of diffraction line shifts for all Laue classes, based on the texture-weighted strain orientation distribution function (WSODF), which is expanded in terms of generalized spherical harmonics.

The strain calculated from the interplanar spacing of the sample under investigation (d) and the reference sample (d_0) is averaged through the rotation for ω around $\mathbf{h} = \mathbf{H}/H$ ($\mathbf{H}$ being a reciprocal lattice vector for the (hkl) plane), which has to be parallel to $\mathbf{y}$, the direction of the diffraction vector in the sample:

$$\langle \varepsilon_{\mathbf{h}}(\mathbf{y}) \rangle = \langle d \rangle / d_0 - 1 \tag{26}$$

Following Popa & Balzar (2001), the strain is given by the following equation:

$$\langle \varepsilon_{\mathbf{h}}(\mathbf{y}) \rangle P_{\mathbf{h}}(\mathbf{y}) = \sum_{l=0}^{\infty} \frac{2}{2l+1} I_l(\mathbf{h}, \mathbf{y}) \tag{27}$$

where the pole distribution functions

$$P_{\mathbf{h}}(\mathbf{y}) = (1/2\pi) \int_0^{2\pi} f(\varphi_1', \Phi_0', \varphi_2') d\omega \tag{28}$$

can be used to calculate the crystallite orientation distribution function $f(\varphi_1, \Phi_0, \varphi_2)$. Here, $(\varphi_1, \Phi_0, \varphi_2)$ are the Euler's angles transforming the sample orthogonal coordinate system $(\mathbf{y}_1, \mathbf{y}_2, \mathbf{y}_3)$ into the crystallite orthogonal coordinate system $(\mathbf{x}_1, \mathbf{x}_2, \mathbf{x}_3)$.

The unit vectors of the directions in crystal and sample, $\mathbf{h}$ and $\mathbf{y}$, are:

$$\mathbf{h} = A_1\mathbf{x}_1 + A_2\mathbf{x}_2 + A_3\mathbf{x}_3 = \cos\beta \sin\Phi \mathbf{x}_1 + \sin\beta \sin\Phi \mathbf{x}_2 + \cos\Phi \mathbf{x}_3 \tag{29}$$

$$\mathbf{y} = \cos\gamma \sin\Psi \mathbf{y}_1 + \sin\gamma \sin\Psi \mathbf{y}_2 + \cos\Psi \mathbf{y}_3 \tag{30}$$

where (Φ, β), (Ψ, γ) are the polar and azimuthal

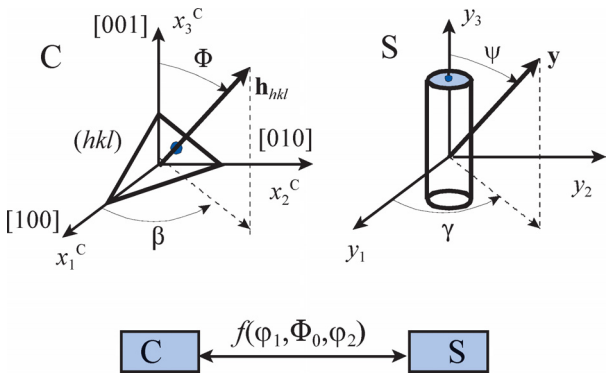

Fig. 2. Relationship between the sample coordinate system S and crystallite coordinate system C.

angles of **h** and **y** in their respective coordinate systems (see Fig. 2).

The harmonic terms $I_l(\mathbf{h},\mathbf{y})$ are defined as:

$$I_l(\mathbf{h},\mathbf{y}) = A_1^2 t_{1l}(\mathbf{h},\mathbf{y}) + A_2^2 t_{2l}(\mathbf{h},\mathbf{y}) + A_3^2 t_{3l}(\mathbf{h},\mathbf{y}) + 2A_2A_3 t_{4l}(\mathbf{h},\mathbf{y}) + 2A_1A_3 t_{5l}(\mathbf{h},\mathbf{y}) + 2A_1A_2 t_{6l}(\mathbf{h},\mathbf{y}) \quad (31)$$

and:

$$t_{il}(\mathbf{h},\mathbf{y}) = A_{il}^0(\mathbf{y})P_l^0(\Phi) + \sum_{m=1}^{l} [A_{il}^m(\mathbf{y})\cos m\beta + B_{il}^m(\mathbf{y})\sin m\beta]P_l^m(\Phi) \quad (32)$$

$$A_{il}^m(\mathbf{y}) = \alpha_{il}^{m0}P_l^0(\Psi) + \sum_{n=1}^{l} (\alpha_{il}^{mn}\cos n\gamma + \beta_{il}^{mn}\sin n\gamma)P_l^n(\Psi)\,,\ (m=0,\,l) \quad (33)$$

$$B_{il}^m(\mathbf{y}) = \gamma_{il}^{m0}P_l^0(\Psi) + \sum_{n=1}^{l} (\gamma_{il}^{mn}\cos n\gamma + \delta_{il}^{mn}\sin n\gamma)P_l^n(\Psi)\,,\ (m=1,\,l) \quad (34)$$

The coefficients α_{il}^{mn}, β_{il}^{mn}, γ_{il}^{mn}, δ_{il}^{mn} can be directly refined in the Rietveld program to yield WSODF and the average strain tensor (Popa & Balzar, 2001). The average stress tensor can also be determined if monocrystal elastic stiffness moduli C_{ij} are known. For a given value of l, the total number of the coefficients for every i is $(2l+1)^2$, where the number l takes only even values because of Friedel's law. If the crystal and sample symmetries are higher than triclinic, the number of coefficients α_{il}^{mn}, β_{il}^{mn}, γ_{il}^{mn}, δ_{il}^{mn} is reduced, some coefficients being zero and some being correlated (detailed analysis for all Laue classes was given by Popa & Balzar (2001)). The required number of refined coefficients to achieve desired precision of WSODF, strain, and stress tensors will depend on the crystal and sample symmetries, as well on the magnitude and gradient of strain and texture.

In cases when finding the WSODF and the average strain and stress tensors is not of interest, one can choose a different approach that corrects only for the line shifts caused by stress. In this case, an alternative representation for I_l is possible with fewer refinable parameters in Rietveld-refinement program. To accomplish this, the orientation angles in the crystal system (Φ, β) are replaced in (32) by the direction cosines (A_1, A_2, A_3). After introducing in (31) and rearranging, one obtains the following expression:

$$I_l(\mathbf{h},\mathbf{y}) = \sum_{k=1}^{k_l} M_{kl}(\Psi,\gamma)J_{k,l+2}(A_1,A_2,A_3) \quad (35)$$

where $J_{k,l+2}$ are homogeneous polynomials of degree $l+2$ in the variables A_1, A_2, A_3, invariant to the Laue class symmetry operations. The functions $M_{kl}(\Psi,\gamma)$ are linear combinations of $A_{il}^m(\Psi,\gamma)$ and $B_{il}^m(\Psi,\gamma)$:

$$M_{kl}(\Psi,\gamma) = \mu_{kl}^0 P_l^0(\Psi) + \sum_{n=1}^{l} (\mu_{kl}^n\cos n\gamma + \nu_{kl}^n\sin n\gamma)P_l^n(\Psi) \quad (36)$$

The coefficients μ_{kl}^n, ν_{kl}^n can be refined in the Rietveld program in the same way as the coefficients α_{il}^{mn}, β_{il}^{mn}, γ_{il}^{mn}, δ_{il}^{mn} from the alternative approach. For sample symmetry higher than triclinic, the coefficients μ_{kl}^n, ν_{kl}^n follow selection rules identical to those for α_{il}^{mn}, β_{il}^{mn}. The maximum number k_l of functions M_{kl} in the series expansion (35) must be equal to or smaller than the total number of functions A_{il}^m, B_{il}^m in (31) and (32), but for crystal symmetry higher than triclinic it is frequently much smaller. For example, for the Laue class $4/m$ and $l=4$, the total number of A_{il}^m, B_{il}^m is 14 but $k_4=8$. This fact is important in Rietveld refinement, as the total number of refinable parameters is kept to a minimum. On the other hand, if this approach is taken, there is no path to obtain WSODF and the average strain and stress tensors from the coefficients μ_{kl}^n, ν_{kl}^n. Therefore, the choice of representation for I_l depends on the problem that we have to solve. An example below uses a hybrid representation in order to accomplish both.

2.3.1. Determination of Texture and Residual-strain Tensor in Cold-rolled Uranium Plate

The neutron TOF diffraction experiments yield the whole diffraction pattern at every sample orientation. A comparable experiment with constant-wavelength neutrons or X-rays would require an order of magnitude longer data collection time in order to scan through a sufficient number of Bragg reflections to determine average strain and stress tensors by this method. The measurements were carried out at the Spectrometer for Materials Research at Temperature and Stress (SMARTS) at the Los Alamos Neutron Science Center (LANSCE), Los Alamos National Laboratory on two uranium plates (plastically deformed by cold rolling and annealed). More experimental details can be found elsewhere (Popa et al., 2005). Texture was determined by GSAS, using the generalized spherical harmonics model (Von Dreele, 1987). It was evident that texture does not conform to *mmm* symmetry, as expected to be produced by rolling. Thus, we have not assumed either texture or strain sample symmetry.

Depending on the crystalline and assumed sample symmetry, as well as on the strength and gradient of strain and texture, it is necessary to inspect (27) for a required number of terms to obtain the desired precision. We determined that for our sample the first three terms suffice:

$$\langle \varepsilon_{\mathbf{h}}(\mathbf{y})\rangle P_{\mathbf{h}}(\mathbf{y}) = 2I_0(\mathbf{h},\mathbf{y}) + \frac{2}{5} I_2(\mathbf{h},\mathbf{y}) + \frac{2}{9} I_4(\mathbf{h},\mathbf{y}) \qquad (37)$$

The harmonic terms $I_l(\mathbf{h},\mathbf{y})$ were used in a hybrid representation because of a fewer number of parameters and the parameters α_{il}^{mn}, β_{il}^{mn}, γ_{il}^{mn}, δ_{il}^{mn}, μ_{kl}^{n}, ν_{kl}^{n} were determined by the least-square refinement by minimizing:

$$\chi^2 = (N-n)^{-1} \times \sum_{i=1}^{N} [(\langle \varepsilon_{\mathbf{h}}(\mathbf{y})\rangle P_{\mathbf{h}}(\mathbf{y}))_{im} - (\langle \varepsilon_{\mathbf{h}}(\mathbf{y})\rangle P_{\mathbf{h}}(\mathbf{y}))_{ic}]^2 / \sigma_i^2 \qquad (38)$$

where N is the number of measured (m) points and n the number of free parameters. For the orthorhombic crystal and triclinic sample symmetry, there were 3 parameters for $l=0$, 45 for $l=2$, and 90 parameters for $l=4$, that is, 138 refinable parameters in total.

The macroscopic strain and stress tensors are obtained from the coefficients for $l=0$, 2 by using the expressions (23) and (24) from Popa & Balzar (2001):

$$\bar{e}_i = \sum_{j=1}^{6} \sum_{k=0}^{25} \overline{w}_{ijk} g_{jk} \qquad (39)$$

$$\bar{s}_i = \sum_{j=1}^{6} \sum_{k=0}^{25} \overline{w}_{ijk} g'_{jk}, \quad g'_{jk} = \sum_{l=1}^{6} C_{jl} \rho_l g_{lk} \qquad (40)$$

Here C_{jl} are the monocrystal elastic stiffness modules; the matrix **w** was given in Table 16 from Popa & Balzar (2001).

Table 3. Strain tensor in sample coordinates for a cold-rolled uranium plate, as determined from the neutron TOF measurements. The figure in parenthesis for $\bar{e}_{11}$ gives standard uncertainty for the two least-significant digits, which is approximately equal for all strain-tensor components. $\bar{e}_{22}$ - rolling direction, $\bar{e}_{11}$ - transverse direction, $\bar{e}_{33}$ - normal direction.

$$\bar{e} = \begin{pmatrix} 1.55\,(22) & -5.41 & -6.16 \\ -5.41 & 6.42 & -0.19 \\ -6.16 & -0.19 & -1.05 \end{pmatrix} \cdot 10^{-4}$$

Table 3 gives the full average strain tensor, as calculated from (39) and (40). As expected, there is a tensile strain in both rolling and transverse directions, about factor of four stronger for the former. This results in the compressive strain in the normal direction of about 10^{-4}. Moreover, shear components are relatively strong. This may be caused by the slipping of rollers during cold rolling and/or significant texture present in the uranium plate before rolling was applied. However, a measurement yielding only strain components along principal sample axes, as customarily carried out, would completely miss this information.

3. Conclusions

Modeling of microstructure in Rietveld refinement programs is discussed with a particular focus on determination of crystallite size distribution and residual strain. A most common Thompson, Cox & Hastings (1987) (TCH) model for diffraction line shapes is discussed and recipes for the extraction of coherently diffracting domain size and strain are given. An example of two CeO_2 powders illustrates cases when Rietveld refinement can give both accurate information about sample microstructure and when it fails due to limitations of the TCH model for describing diffraction line profiles. Furthermore, two models for accounting for diffraction line shifts due to residual stress were reviewed. It was illustrated how the model based on an expansion of texture-weighted strain orientation distribution function in terms

of generalized spherical harmonics can be used to evaluate the average macroscopic strain tensor in a cold rolled uranium plate. A methodology for an orthorhombic crystal symmetry and general triclinic sample symmetry was presented and all six components of the average strain tensor were calculated, based on the neutron TOF measurements collected at the SMARTS instrument at LANSCE.

Acknowledgements

We gratefully acknowledge Nathalie Audebrand and Daniel Louër (University of Rennes) for preparing and instrument scientists at seven facilities for carrying out the measurements on the Size Strain Round Robin CeO_2 powder, and the Commission on Powder Diffraction (CPD) of the International Union of Crystallography (IUCr) for supporting the Size-Strain Round Robin.

References

Audebrand, N., Auffrédic, J.-P. & Louër, D. (2000). *Chem. Mater.* **12**, 1791–1799.

Balzar, D. (1999). In *Defect and Microstructure Analysis by Diffraction*, edited by R. Snyder, J. Fiala & H. J. Bunge, pp. 94–126. IUCr/Oxford University Press.

Balzar, D., Audebrand, N., Daymond, M., Fitch, A., Hewat, A., Langford, J. I., Le Bail, A., Louër, D., Masson, O., McCowan, C. N., Popa, N. C., Stephens, P. W. & Toby, B. (2004). *J. Appl. Cryst.* **37**, 911–924.

Balzar, D. & Ledbetter, H. (1993). *J. Appl. Cryst.* **26**, 97–103.

Balzar, D. & Ledbetter, H. (1995). *Adv. X-ray Analysis* **38**, 397–404.

Balzar, D., Von Dreele, R. B., Bennett, K. & Ledbetter, H. (1998). *J. Appl. Phys.* **84**, 4822–4833.

Behnken, H. (2000). *Phys. Stat. Sol. (a)* **177**, 401–418.

Berkum, J. G. M. van (1994). Ph.D. Thesis, Delft University of Technology, p. 136.

Bertaut, E. F. (1949). *C. R. Acad. Sci. Paris* **228**, 187–189.

Bunge, H. J. (1982). *Texture Analysis in Material Science*. London: Butterworth.

Cagliotti, G., Paoletti, A. & Ricci, F. P. (1958). *Nucl. Instrum. Methods* **3**, 223–228.

Christenson, A. L. & Rowland, E. S. (1953). *Transactions ASM* **45**, 638–676.

Daymond, M. R., Bourke, M. A. M., Von Dreele, R. B., Clausen, B. & Lorentzen, T. (1997). *J. Appl. Phys.* **82**, 1554–1562.

Dollase, W. A. (1986). *J. Appl. Cryst.*, **19**, 267–272.

Ferrari, M. & Lutterotti, L. (1994). *J. Appl. Phys.* **76**, 7246–7255.

Guinier, A. (1963). *X-Ray Diffraction*, p. 139. San Francisco: Freeman.

Hauk, V. (1952). *Arch. f. d. Eisenhüttenwesen* **23**, 353–361.

Hauk, V. (1997). *Structural and Residual Stress Analysis by Nondestructive Methods*. Amsterdam: Elsevier.

Howard, S. A. & Preston, K. D. (1989). In *Modern Powder Diffraction*, Vol. 20, edited by D. L. Bish and J. E. Post, pp. 217–275. Washington, D.C.: The Mineralogical Society of America.

Klug, H. P. & Alexander, L. E. (1974). *X-ray Diffraction Procedures*, 2nd ed. New York: John Wiley.

Krill, C. E. & Birringer, R. (1998). *Philos. Mag.* **A77**, 621–640.

Langford, J. I. (1978). *J. Appl. Cryst.* **11**, 10–14.

Langford, J. I., Louër, D. & Scardi, P. (2000). *J. Appl. Cryst.* **33**, 964–974.

Larson, A. C. & Von Dreele, R. B. (2001). *General Structure Analysis System GSAS*, Los Alamos National Laboratory Report.

Lutterotti, L. (1998). http://www.ing.unitn.it/~luttero/maud/index.html.

Matthies, S., Lutterotti, L. & Wenk, H. R. (1997). *J. Appl. Cryst.* **30**, 31.

Noyan, I. C. & Cohen, J. B. (1987). *Residual Stress*. New York: Springer-Verlag.

Popa, N. C. (1992). *J. Appl. Cryst.* **25**, 611–616.

Popa, N. C. (1998). *J. Appl. Cryst.* **31**, 176–180.

Popa, N. C. & Balzar, D. (2001). *J. Appl. Cryst.* **34**, 187–195.

Popa, N. C. & Balzar, D. (2002). *J. Appl. Cryst.* **35**, 338–346.

Popa, N C., Balzar, D., Stefanic, G., Vogel, S., Brown, D., Bourke, M., Clausen, B. (2005). *Advances in X-Ray Analysis* **47**, CD-ROM.

Reuss, A. (1929). *Z. Angew. Math. Mech.* **9**, 49–58.

Rietveld, H. (1969). *J. Appl. Cryst.* **2**, 65–71.

Scardi, P. & Leoni, M. (2001). *Acta Cryst.* **A57**, 604–613.

Scardi, P. & Leoni, M. (2002), *Acta Cryst.* **A58**, 190–200.

Scherrer, P. (1918). *Nachr. Gött.* **2**, 98–100.

Smith, W. L. (1976). *J. Appl. Cryst.* **9**, 187–189.

Stephens, P. W. (1999). *J. Appl. Cryst.* **32**, 281–288.

Stokes, A. R. & Wilson, A. J. C. (1944). *Proc. Phys. Soc. (Lond.)* **56**, 174–181.

Thompson, P., Cox, D. E. & Hastings, J. B. (1987). *J. Appl. Cryst.* **20**, 79–83.

Ungár, T., Gubicza, J., Ribárik, G. & Borbély, A. (2001). *J. Appl. Cryst.* **34**, 298–310.

Von Dreele, R. B. (1997). *J. Appl. Cryst.* **30**, 517–525.

Wang, Y. D., Peng, R. L. & McGreevy, R. L. (1999). *Proceedings of the Twelfth International Conference on Textures of Materials ICOTOM-12, Canada, August 9–13*, pp. 553–559.

Wang, Y. D., Peng, R. L., Zeng, X. H. & McGreevy, R. L. (2000). *Mater. Sci. Forum* **347–349**, 66–73.

Warren, B. E. (1969). *X-Ray Diffraction*, pp. 251–314. New York: Addison-Wesley.

York, B. R. (1997). *Adv. X-Ray Anal.* **41**, 544–555.

Young, R. A. and Desai, P. (1989). *Arch. Nauk Mater.* **10**, 71–90.